

A more accurate projection in the rate-controlled constrained-equilibrium method for dimension reduction of combustion chemistry

Qing Tang¹ and Stephen B Pope

Sibley School of Mechanical and Aerospace Engineering, Cornell University, Ithaca, NY 14853, USA

E-mail: qtang@mae.cornell.edu

Received 20 June 2003, in final form 5 February 2004

Published 19 March 2004

Online at stacks.iop.org/CTM/8/255 (DOI: 10.1088/1364-7830/8/2/004)

Abstract

The rate-controlled constrained-equilibrium (RCCE) method for dimension reduction of combustion chemistry is revisited from a geometric viewpoint. A constrained equilibrium manifold (CEM) is defined as all compositions that satisfy the maximum-entropy or minimum-free energy conditions of the gas mixture, subject to specified constraints. The RCCE method is based solely on thermodynamics, and it is shown that this method contains a hidden assumption of an orthogonal projection that projects the rate equation of the chemical system onto the CEM. An extension of the RCCE method is constructed by making an alternative projection based on the conjecture that, near the CEM, there is a close parallel inertial manifold (CPIM). The CPIM assumption introduces the chemical kinetics directly through the local Jacobian and hence leads to greater accuracy than RCCE. The comparison between the RCCE method and its extension is made in the test calculations of hydrogen–air and methane–air autoignition.

1. Introduction

To make feasible calculations of turbulent combustion with realistic chemistry, it is necessary to reduce the computational cost of solving the complex thermo-chemical system. There are basically two strategies for achieving this goal, namely dimension reduction and storage/retrieval.

The aim of dimension reduction strategies is to represent the chemistry accurately in terms of a relatively small number, n_c , of reduced variables $\mathbf{c} = \{c_1, c_2, \dots, c_{n_c}\}$, instead of directly in terms of the n_s species moles $\mathbf{N} = \{N_1, N_2, \dots, N_{n_s}\}$. Then, in the turbulent combustion

¹ Present address: Reaction Engineering International, Salt Lake City, UT 84101, USA.

calculation, the relevant equations are solved for the n_c reduced variables instead of for the n_s species. Since the computational cost increases at least linearly with the number of variables represented, substantial gains can be achieved for $n_c \ll n_s$.

It is informative to take a geometric view of dimension reduction. An implication of the dimension reduction assumption is that the species moles are known in terms of the reduced variables, i.e.

$$N = N^m(\mathbf{c}), \quad (1)$$

where the function $N^m(\mathbf{c})$ defines an n_c -dimensional manifold (parametrized by \mathbf{c}) in the n_s -dimensional species space. The dimension reduction assumptions can be thought of as the imposition of $n_R \equiv n_s - n_c$ conditions that determine N^m .

In the past, a number of dimension reduction methods have been introduced. Many of them are based on the observation that, in a typical combustion system, there is a wide range of timescales present in the chemical mechanism. The very fast timescales are usually associated with local equilibrium processes, while the long-term dynamics of the combustion system are determined by a small number of slow processes, at least after the decay of transients. From a geometric point of view, these slow processes can be described by a finite-dimensional attractor of a lower dimension than the full species space (Tomlin *et al* 1997). The attractor is embedded in the so-called inertial manifold \mathcal{M} , which is attracting, invariant and smooth. In other words, the reaction trajectory from any point in the manifold remains in the manifold. For inertial manifolds, the rate-of-change of the reduced variables is determined by the full chemical kinetics without approximation. The existing dimension reduction approaches based on timescale analysis of the chemical reaction system are distinguished from each other by their strategies to approximate or evaluate directly the inertial manifold \mathcal{M} . Some of the most prominent dimension reduction methods that fall into this category are the reduction technique based on the quasi-steady-state assumption (QSSA) (Bodenstein and Lind 1906, Peters and Williams 1987, Smooke 1991), the intrinsic low-dimensional manifold (ILDM) approach (Maas and Pope 1992) and the rate-controlled constrained equilibrium (RCCE) method (Keck and Gillespie 1971, Keck 1990).

The second strategy for efficient implementation of combustion chemistry is storage/retrieval. In a typical turbulent combustion calculation, the combustion chemistry has to be computed at least 10^9 times, e.g. on each of 1000 iterations (or time steps) for each of 1000 000 cells (or particles). The idea of storage/retrieval is to avoid performing these expensive chemistry calculations 10^9 times but instead to store the information from many fewer calculations and then (when possible with sufficient accuracy) to retrieve the information 10^9 times. Several efficient storage/retrieval methods have been developed in recent years. We mention the piecewise reusable implementation of solution mapping (PRISM) with quadratic polynomials (Tonse *et al* 1999) and the *in situ* adaptive tabulation (ISAT) (Pope 1997), which directly take advantage of the intrinsic sparseness in the species space. Other approaches require samplings of the chemical kinetic states within the anticipated combustion regimes prior to the simulation and then fit the sampled chemical states by various means, such as the method using artificial neural networks (Blasco *et al* 2000), repro-modelling using orthogonal polynomials (Turányi 1994) and high-dimensional model representations (HDMRs) (Li *et al* 2001).

The computational cost of using the detailed chemical information in turbulent combustion simulations can be dramatically reduced by exploiting, in combination, techniques of dimension reduction and storage/retrieval. For example, recent PDF calculations of turbulent methane flames (Tang *et al* 2000) have used a 19-species reduced mechanism (Sung *et al* 2001), implemented using ISAT. These two measures reduce the computational cost—compared with

the direct use of the detailed mechanism—by at least a factor of 1000, making feasible, in days of computer time, calculations that otherwise would have taken years.

Recently, efforts have been made to develop more general and unified dimension reduction/ISAT methodologies (Tang and Pope 2002) as opposed to the previous ISAT-QSSA approach (Tang *et al* 2000), where the reduction (QSSA) and tabulation (ISAT) are separate and are implemented using separate computer programs. It is important to appreciate the crucial role played by the low-dimension manifolds in the implementation of dimension reduction in combination with ISAT. Among the desirable properties of such manifolds are: existence and uniqueness (for every valid reduced composition \mathbf{c}), continuity and smoothness, local determination and being inertial. Approaches such as QSSA, RCCE and ILDM are ‘local’ in the sense that, given a particular reduced composition, the corresponding point on the manifold can be determined without constructing the whole manifold and hence are more easily applied in higher dimensions and are more naturally combined with ISAT. However, our experience with QSSA and ILDM has indicated that the low-dimension manifolds implied by both methods are not everywhere continuous and differentiable. A discussion about the discontinuity of the ILDMs can also be found in Nafe and Maas (2002). This led us to RCCE, where the constrained equilibrium manifolds (CEMs) have excellent mathematical properties: they exist for all realizable \mathbf{c} ; they are unique; and they are infinitely differentiable (at least in the interior of the realizable region) (Pope 2004).

Unlike QSSA and ILDM, which are appropriately based on dynamical-systems approaches to the chemical kinetics, RCCE is solely based on thermodynamics. Its ‘efficiency’ is questionable since it is not clear that the implied reduction assumption is near optimal. It should also be pointed out that none of the above methods generates inertial manifolds and hence the rate-of-change of the reduced variables depends strongly on the choice of the projection used to project the full rate-of-change vector onto the manifolds (see, e.g. Maas and Pope 1992).

In this paper, we report our progress in developing the ISAT-RCCE approach, while the focus is on improving the accuracy of RCCE while maintaining the superior mathematical properties of the CEM. The remainder of this paper is organized as follows. A brief description of the RCCE method is provided first. In the next section we show that there is a hidden reduction assumption in RCCE (i.e. an orthogonal projection), which projects the rate equation of the chemical system onto the CEM. An alternative projection and its implementation in terms of Lagrange multipliers are then proposed. The comparison between the RCCE method and its extension is made in the test calculations of hydrogen–air and methane–air autoignition. Conclusions are drawn in the final section.

2. Rate-controlled constrained-equilibrium

The RCCE method was introduced by Keck and Gillespie (1971); it was reviewed by Keck (1990), and some recent advances can be found in the literature (e.g. Hamiroune *et al* 1998, Yousefian 1998). In this method, it is assumed, as in thermodynamics, that fast reactions exist that relax the chemical system to the associated constrained equilibrium state on a timescale shorter than that on which the constraints are changing. In other words, a non-equilibrium system will relax to its final equilibrium state through a sequence of RCCE states.

We now consider the constrained equilibrium state of an ideal gas mixture with n_s species and n_e elements. First the species space \mathcal{S} is defined to be the real n_s -dimensional Euclidean space with orthonormal basis vectors $\mathbf{e}_i, i = 1, \dots, n_s$. Thus, the species moles are represented

by the vector

$$N \equiv \mathbf{e}_i N_i, \quad (2)$$

where the summation convention applies.

Three types of constraints are used to define the constrained equilibrium state.

(i) There are constraints on the moles of n_{cs} specified species, which can be written

$$(\mathbf{S}^c)^T N = N^c, \quad (3)$$

where \mathbf{S}^c is an $n_s \times n_{cs}$ matrix, every column of which is zero, except for a 1 in the row corresponding to a constrained species, and the corresponding row of N^c is the specified number of moles of that species.

(ii) There are n_e constraints on the moles of elements, which can be written

$$\mathbf{E}^T N = N^e, \quad (4)$$

where N^e is specified, and \mathbf{E} is an $n_s \times n_e$ matrix, whose general component, E_{ij} , denotes the number of atoms of element j in one molecule of species i .

(iii) There are n_g general linear constraints ($n_g \geq 0$), which are written

$$(\mathbf{B}^g)^T N = \mathbf{c}^g. \quad (5)$$

The total number of constraints is $n_c \equiv n_{cs} + n_e + n_g$. These are combined into the constraint equation

$$\mathbf{B}^T N = \mathbf{c}, \quad (6)$$

where the $n_s \times n_c$ constraint matrix \mathbf{B} is

$$\mathbf{B} = [\mathbf{S}^c \mathbf{E} \mathbf{B}^g] \quad (7)$$

and the n_c constraint vector \mathbf{c} is

$$\mathbf{c} = [(N^c)^T (N^e)^T (\mathbf{c}^g)^T]^T. \quad (8)$$

In RCCE, it is necessary that the constraints be linearly independent: thus matrix \mathbf{B} must have full column rank. The n_c -dimensional constraint subspace \mathcal{B} is defined as $\mathcal{B} \equiv \text{span}(\mathbf{B})$.

In addition to the specified constraints, the constrained equilibrium state depends on two thermodynamic state variables. Specifically, if pressure, p , and enthalpy, H , are specified, the constrained equilibrium composition is defined to be that which maximizes the entropy $S(N, p, H)$ subject to n_c constraints—equation (6). The n_R implied dimension-reduction conditions can be written

$$(\mathbf{B}^\perp)^T \nabla S = 0, \quad (9)$$

where ∇ represents the gradient of entropy in the species space and the n_R columns of \mathbf{B}^\perp span the orthogonal complement of the constraint subspace spanned by the columns of \mathbf{B} . Thus a CEM can be defined as all compositions N satisfying the (constrained) maximum-entropy condition equation (9); and the CEM is parametrized by the constraint vector \mathbf{c} . If, on the other hand, pressure, p , and temperature, T , are specified, then the constrained equilibrium composition minimizes the Gibbs free energy, G , and the CEM can be defined similarly.

To calculate the constrained equilibrium state at fixed p and T , we define the normalized Gibbs function as

$$\tilde{G} = N_i [\tilde{g}_i(T, p) + \ln X_i], \quad (10)$$

where the summation convention applies, and X_i is the mole fraction of species i . The normalized specific Gibbs function is

$$\tilde{g}_i = \frac{h_i}{\mathcal{R}T} - \frac{s_i^0}{\mathcal{R}} + \ln \left(\frac{p}{p_{\text{atm}}} \right), \quad (11)$$

where h_i and s_i^0 are the specific enthalpy and the standard state molar entropy for species i , respectively, \mathcal{R} is the universal gas constant and p_{atm} is the standard state pressure.

At fixed temperature, T , and pressure, p , and given the constraint matrix \mathbf{B} and the constraint vector \mathbf{c} , the constrained equilibrium composition N^{CE} is the species moles vector N that satisfies the constraint equation, equation (6), and minimizes the Gibbs function, \tilde{G} , equation (10). N^{CE} can be found easily using the elegant method of undetermined Lagrange multipliers (Reynolds 1986). The solution proposed by Lagrange involves finding the unconstrained minimum of the function

$$\begin{aligned}\tilde{G} &\equiv \tilde{G} - \sum_{j=1}^{n_c} \lambda_j (B_{ij} N_i - c_j) \\ &= \tilde{G} - \boldsymbol{\lambda}^T (\mathbf{B}^T N - \mathbf{c}),\end{aligned}\quad (12)$$

where $\boldsymbol{\lambda}$ is the $n_c \times 1$ vector of Lagrange multipliers, or constraint potentials. At the minimum of the extended function \tilde{G} , we have the condition

$$d\tilde{G} = 0 \quad (13)$$

or

$$(\tilde{g}_i + \ln X_i - B_{ij} \lambda_j) dN_i + \bar{N} \sum_{i=1}^{n_s} dX_i - (B_{ij} N_i - c_j) d\lambda_j = 0, \quad (14)$$

where $\bar{N} \equiv \sum_{i=1}^{n_s} N_i$ is the total number of moles of species and $X_i = N_i/\bar{N}$. The last two terms on the left-hand side of equation (14) are zero because the species mole fractions sum to unity and because the multiplier of $d\lambda_j$ is zero. Thus, the equilibrium condition becomes

$$(\ln X_i + \tilde{g}_i - B_{ij} \lambda_j) dN_i = 0. \quad (15)$$

The multiplier of dN_i must also be zero (where \tilde{G} is minimum), leading to

$$X_i = \exp(-\tilde{g}_i + B_{ij} \lambda_j) \quad (16)$$

or, equivalently,

$$\mathbf{X} = \exp(-\tilde{\mathbf{g}} + \mathbf{B}\boldsymbol{\lambda}). \quad (17)$$

Thus we have the important result that, in the constrained equilibrium state, the n_s species mole fractions \mathbf{X} are determined in terms of n_c Lagrange multipliers $\boldsymbol{\lambda}$ by equation (17).

To summarize, at fixed T and p , the constrained equilibrium composition N^{CE} , the constraints \mathbf{c} , and the Lagrange multipliers $\boldsymbol{\lambda}$ are related by the following $n_c + 1$ non-linear equation system

$$\bar{N} \mathbf{B}^T \mathbf{X} = \mathbf{c} \quad (18)$$

and

$$\sum_{i=1}^{n_s} X_i = \sum_{i=1}^{n_s} N_i/\bar{N} = 1, \quad (19)$$

where

$$\mathbf{X} = \exp(-\tilde{\mathbf{g}} + \mathbf{B}\boldsymbol{\lambda}) \quad (20)$$

and

$$N^{\text{CE}} = \bar{N} \exp(-\tilde{\mathbf{g}} + \mathbf{B}\boldsymbol{\lambda}). \quad (21)$$

Equations (18) and (19) can be solved for the $n_c + 1$ unknowns $\boldsymbol{\lambda}$ and \bar{N} , and then the constrained equilibrium composition N^{CE} is obtained using equation (21).

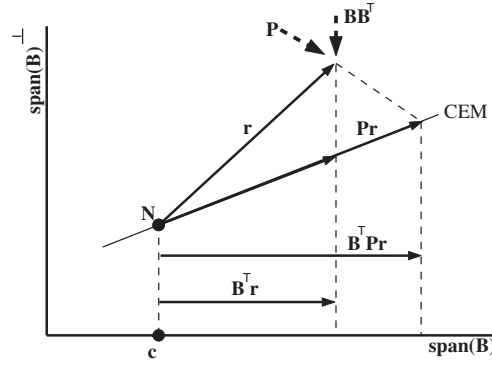


Figure 1. Sketch of the CEM in the species space (represented by the constraint subspace \mathcal{B} and the unrepresented subspace $\mathcal{U} = \mathcal{B}^\perp$). For simplicity the CEM is shown as being plane.

For fixed H and p , the above equation system still holds, while in solving for the constrained equilibrium composition, an iterative calculation is performed to adjust T and X to satisfy the condition of constant H . More detailed descriptions of this method can be found in the literature (e.g. Reynolds 1986, Gordon and McBride 1994, Bishnu *et al* 1997, Pope 2004).

3. Projections in the RCCE method

For a homogeneous system consisting of a reacting ideal gas mixture, the evolution of the species compositions can be described by the rate equation of species,

$$\dot{N} = \frac{dN}{dt} = r. \quad (22)$$

The $n_s \times 1$ vector r represents the rate-of-change due to reaction, which can be evaluated using a detailed chemical mechanism.

We now show that there is a hidden assumption (of an orthogonal projection) in the RCCE method. The constraint equation, equation (6), is

$$c = \mathbf{B}^T N^{\text{CE}}, \quad (23)$$

from which the RCCE evolution equation, the rate equation of constraints,

$$\dot{c} = \mathbf{B}^T \dot{N}^{\text{CE}} = \mathbf{B}^T r, \quad (24)$$

appears to follow without assumption (since the constraint matrix \mathbf{B} is independent of time). In the RCCE method, the dimension reduction of the reacting system is achieved by integrating equation (24) instead of equation (22), and it should be noted that r in equation (24) must be evaluated on the CEM.

A geometric view of the problem exposes a hidden assumption. Figure 1 shows a sketch of the CEM in the n_s -dimensional species space. This space is represented in the sketch by an axis $\text{span}(\mathbf{B})$ for the constraint subspace \mathcal{B} , and an axis $\text{span}(\mathbf{B})^\perp$ for the unrepresented subspace \mathcal{U} . The sketch shows the rate-of-change vector r at the general point N on the CEM. An important observation is that r is not in the tangent space of the CEM, and so (for infinitesimal dt), $N + \dot{N} dt = N + r dt$ is not on the CEM since in general the CEM is not an inertial manifold. However, by assumption all represented compositions lie on the manifold, and hence it is necessary to project r onto the manifold. With \mathbf{P} denoting the projection, the sketch shows that $\mathbf{P}r$ is in the tangent space of the CEM.

To achieve dimension reduction, we wish to represent the process in the constraint subspace, which is accomplished by projecting orthogonally onto \mathcal{B} , yielding

$$\dot{\mathbf{c}} = \mathbf{B}^T \mathbf{P} \dot{\mathbf{N}} = \mathbf{B}^T \mathbf{P} \mathbf{r}. \quad (25)$$

Both from the sketch and by comparing equation (24) and equation (25), it may be seen that RCCE contains the hidden assumption that \mathbf{P} is a projection onto the CEM in the unrepresented subspace and hence perpendicular to the constraint subspace. It is well appreciated (e.g. from ILDM theory) that the appropriate projection is in the fast subspace, which could be very different from the projection implied by the RCCE method: the fast subspace is spanned by the eigenvectors corresponding to the eigenvalues with the smallest real parts of the local Jacobian matrix and is generally not the fixed unrepresented subspace \mathcal{U} .

4. Close parallel inertial manifold

One way of improving the accuracy of RCCE is to reconstruct the rate-of-change vector in the CEM to better approximate the accurate rate-of-change vector in the slow manifold. To achieve this goal, an alternative projection in RCCE is formed by considering a hypothesized inertial manifold that is close to the CEM and parallel to it. We refer to it as the close parallel inertial manifold (CPIM).

We first introduce the concept of the tangent subspace of the CEM in more detail by completing the species space \mathcal{S} decomposition. The unrepresented subspace \mathcal{U} is defined as the orthogonal complement of \mathcal{B} —the constraint subspace. It has dimension $n_u = n_R = n_s - n_c$. Let the columns of the $n_s \times n_u$ matrix \mathbf{U} provide an orthonormal basis for \mathcal{U} . Then for a given constraint vector \mathbf{c} , all composition vectors in space \mathcal{S} that satisfy $\mathbf{B}^T \mathbf{N} = \mathbf{c}$ can be expressed as

$$\mathbf{N} = \mathbf{N}^{\text{CE}}(\mathbf{c}) + \mathbf{U} \delta \mathbf{u}, \quad (26)$$

where $\delta \mathbf{u}$ is an n_u -vector and $\mathbf{N}^{\text{CE}}(\mathbf{c})$ is the corresponding constrained equilibrium composition.

The n_c -dimensional tangent space of the CEM at \mathbf{c} , denoted by $\mathcal{T}(\mathbf{c})$, is that spanned by the n_c vectors

$$\hat{\mathbf{t}}_j \equiv \frac{\partial \mathbf{N}^{\text{CE}}(\mathbf{c})}{\partial c_j}, \quad j = 1, 2, \dots, n_c \quad (27)$$

and the $n_s \times n_c$ tangent space matrix $\hat{\mathbf{T}}$ is formed as

$$\hat{\mathbf{T}} = [\hat{\mathbf{t}}_1 \hat{\mathbf{t}}_2 \cdots \hat{\mathbf{t}}_{n_c}]. \quad (28)$$

An expression for $\hat{\mathbf{T}}$ in terms of \mathbf{B} , \mathbf{N}^{CE} and \mathbf{c} for fixed H and p is given in appendix A. A unitary matrix $\mathbf{T} = [\mathbf{t}_1 \mathbf{t}_2 \cdots \mathbf{t}_{n_c}]$ can always be found such that $\text{span}(\hat{\mathbf{T}}) = \text{span}(\mathbf{T})$. The n_u -dimensional normal subspace $\mathcal{N}(\mathbf{c})$ is defined as the orthogonal complement of $\mathcal{T}(\mathbf{c})$. Let the column vectors of an $n_s \times n_u$ unitary matrix $\mathbf{\Omega}$ span the normal subspace. Then the column vectors in \mathbf{T} and $\mathbf{\Omega}$ provide another basis for the species space \mathcal{S} . Any vector \mathbf{s} in \mathcal{S} has a representation

$$\mathbf{s} = \mathbf{T} \mathbf{s}_T + \mathbf{\Omega} \mathbf{s}_N, \quad (29)$$

where $\mathbf{s}_T = \mathbf{T}^T \mathbf{s}$ are the components in the tangent plane and $\mathbf{s}_N = \mathbf{\Omega}^T \mathbf{s}$ are those in the normal subspace.

Another important concept is the local Jacobian matrix $\mathbf{J}(\mathbf{N})$, which is $n_s \times n_s$ with elements

$$J_{ij} \equiv \frac{\partial r_i}{\partial N_j}. \quad (30)$$

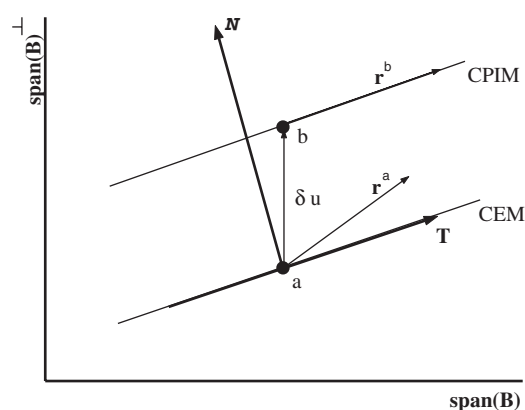


Figure 2. Sketch of the CPIM and the CEM in the species space (represented by the constraint subspace \mathcal{B} and the unrepresented subspace $\mathcal{U} = \mathcal{B}^\perp$). For simplicity, the manifolds are shown as being plane.

The eigenvalues of \mathbf{J} characterize the timescales associated with the reactive system. Also notice that for an infinitesimal change of the composition vector δN , the rate-of-change vector can be expressed as

$$\mathbf{r}(N + \delta N) = \mathbf{r}(N) + \mathbf{J}(N)\delta N. \quad (31)$$

Figure 2 shows the sketch of the CPIM together with the CEM in the species space (represented by the constraint subspace \mathcal{B} and the unrepresented subspace \mathcal{U}). In the sketch the point (a) is on the CEM, with the composition being N^a and the rate-of-change vector \mathbf{r}^a . The tangent space of the CEM and its normal subspace are denoted by \mathbf{T} and \mathbf{N} , respectively. The point (b) lies on the CPIM, with the composition being N^b , which satisfies the condition

$$\mathbf{B}^T N^b = \mathbf{B}^T N^a \quad (32)$$

and \mathbf{r}^b is the reconstructed rate-of-change vector.

As discussed in the introduction section, the philosophy behind most of the dimension reduction methods based on timescale separation is to use some means to approximate the inertial manifolds that represent the slow chemistry. Previous studies on the RCCE method (see, e.g. Keck 1990, Hamiroune *et al* 1998) have demonstrated the capability of RCCE of achieving a high accuracy in dimension reduction of combustion chemistry. Here we claim that, when the RCCE method ‘works’, the CEM must be a good approximation to the slow inertial manifolds or in other words be close to and approximately parallel to the slow inertial manifolds. The speculation of the CEM being parallel to the slow manifold stems from the observation that in practice most of the major species (i.e. fuel, oxidant and major combustion products) are selected to form the constraints in RCCE, and therefore both the slow manifolds and the CEM (parametrized by the constraints) are only allowed to vary within a very narrow range in the unrepresented subspace in terms of the ‘unrepresented’ species mass fraction. The above hypothesis forms the foundation of the CPIM methodology: first, if the slow manifolds are close to the CEM, the accurate rate-of-change vector can be better approximated by \mathbf{r}^b , obtained by first-order Taylor series expansion of \mathbf{r}^a using equation (31), which involves the local Jacobian and hence the chemical kinetics; and second, if the inertial slow manifolds are approximately parallel to the CEM, vector \mathbf{r}^b should be in the tangent space of the CEM. The rest of this section describes the procedure for constructing \mathbf{r}^b .

We start from the difference between N^b and N^a , which lies entirely in the subspace \mathcal{U} , and can be expressed as

$$\delta N \equiv N^b - N^a = \mathbf{U}\delta u. \quad (33)$$

For given N^a and N^b , the above equation defines δu uniquely. By the inertial manifold assumption, the components of r^b in the normal subspace \mathcal{N} should be zero:

$$(r^b)_N = \Omega^T r^b = 0. \quad (34)$$

Using the linear approximation, equation (31), we have

$$r^b = r(N^b) = r^a + \mathbf{J}(N^b - N^a) = r^a + \mathbf{J}\mathbf{U}\delta u. \quad (35)$$

Thus, equation (34) yields

$$\Omega^T r^b = 0 = \Omega^T r^a + \Omega^T \mathbf{J}\mathbf{U}\delta u \quad (36)$$

and hence

$$\delta u = -\mathbf{K}^{-1}\Omega^T r^a, \quad (37)$$

where the $n_u \times n_u$ matrix \mathbf{K} is

$$\mathbf{K} = \Omega^T \mathbf{J}\mathbf{U}. \quad (38)$$

The appearance of the inverse \mathbf{K}^{-1} in equation (37) raises questions of singularity that are addressed in the next section. Substituting equation (37) into equation (35), we obtain r^b in the CPIM in terms of r^a ,

$$r^b = r^a + \mathbf{J}\mathbf{U}\delta u = (\mathbf{I} - \mathbf{J}\mathbf{U}\mathbf{K}^{-1}\Omega^T)r^a = \mathbf{T}\mathbf{T}^T(\mathbf{I} - \mathbf{J}\mathbf{U}\mathbf{K}^{-1}\Omega^T)r^a. \quad (39)$$

The product $\mathbf{T}\mathbf{T}^T$ defines an orthogonal projection onto \mathcal{T} . Since r^b lies in the tangent subspace, $\mathbf{T}\mathbf{T}^T r^b = r^b$ and the last step in equation (39) follows. The difference between r^b and r^a can be viewed in two parts: first, the removal of the normal component, yielding $\mathbf{T}\mathbf{T}^T r^a$; and second, a modification to the tangential component, i.e. the addition of $-\mathbf{T}\mathbf{T}^T \mathbf{J}\mathbf{U}\mathbf{K}^{-1}\Omega^T r^a$. Note that the first modification amounts to the perpendicular projection of r^a onto \mathcal{T} and is well-conditioned independent of \mathbf{K} .

Using the sketch shown in figure 2, the projection implied by the CPIM assumption is

$$\mathbf{P} = \mathbf{I} - \mathbf{J}\mathbf{U}\mathbf{K}^{-1}\Omega^T \quad (40)$$

and the rate equation of constraints using CPIM becomes

$$\dot{c} = \mathbf{B}^T \mathbf{P}r, \quad (41)$$

where r is evaluated on the CEM.

5. A realizable implementation of CPIM

So far we have developed the methodology of CPIM, which can be viewed as an extension to the original RCCE method and has the potential to improve the dimension-reduction accuracy. However, to make the approach robust and physically sound, two realizability issues need to be addressed:

- (i) the matrix \mathbf{K} in equation (38) may be ill-conditioned;
- (ii) the rate-of-change vector $\mathbf{P}r$ in equation (41) may lead to negative entropy production.

These issues stem from the fact that the CPIM is not purely determined by a chemical mechanism, and realizability violations usually take place when a ‘bad’ constraint subspace is chosen and/or at certain thermodynamic regimes (e.g. low temperature region) where the CEM is far from the slow inertial manifold.

A stable inverse of matrix \mathbf{K} is introduced to address the first issue. Let the SVD of \mathbf{K} be

$$\mathbf{K} = \mathbf{\Omega}^T \mathbf{J} \mathbf{U} = \mathbf{W} \mathbf{\Sigma} \mathbf{V}^T, \quad (42)$$

where the matrix of singular values is

$$\mathbf{\Sigma} = \text{diag}(\sigma_1, \sigma_2, \dots, \sigma_{n_u}). \quad (43)$$

We now replace $\mathbf{\Sigma}^{-1}$ by

$$\tilde{\mathbf{\Sigma}} \equiv \text{diag} \left(\frac{1}{\sigma_1 + \zeta \sigma_1}, \frac{1}{\sigma_2 + \zeta \sigma_1}, \dots, \frac{1}{\sigma_{n_u} + \zeta \sigma_1} \right), \quad (44)$$

where ζ is a small positive parameter ($\zeta = 1.0 \times 10^{-8}$ in this study). Thus the pseudo-inverse of \mathbf{K} ,

$$\tilde{\mathbf{K}} \equiv \mathbf{V} \tilde{\mathbf{\Sigma}} \mathbf{W}^T, \quad (45)$$

is well-conditioned and is used in place of \mathbf{K}^{-1} in equation (37).

The entropy on the CEM is denoted by S^{CEM} . The rate-of-change of entropy at fixed enthalpy H and pressure p is

$$\dot{S}^{\text{CEM}} = \frac{\partial S}{\partial N_i^{\text{CE}}} \dot{N}_i^{\text{CE}} = (\nabla S)^T \mathbf{r}. \quad (46)$$

The fact that the entropy production rate, \dot{S}^{CEM} , on CEM is non-negative has been shown by Keck (1990). The entropy production rate on the CPIM S^{CPIM} can be expressed as

$$\dot{S}^{\text{CPIM}} = (\nabla S)^T \mathbf{P} \mathbf{r}. \quad (47)$$

We define γ as the ratio of the entropy production rates generated by CPIM and RCCE, respectively:

$$\gamma \equiv \frac{\dot{S}^{\text{CPIM}}}{\dot{S}^{\text{CEM}}}. \quad (48)$$

Note that γ can be negative because of the infeasible CPIM. To avoid this problem, a blending of \mathbf{r} and $\mathbf{P} \mathbf{r}$ is used:

$$\tilde{\mathbf{r}} = \alpha \mathbf{P} \mathbf{r} + (1 - \alpha) \mathbf{r}, \quad (49)$$

where the blending factor, α , is a number between 0 and 1. Then, with $\tilde{\mathbf{r}}$ used in place of $\mathbf{P} \mathbf{r}$ in equation (41), the ratio of entropy production rates is

$$\tilde{\gamma} = \alpha \gamma + 1 - \alpha \quad (50)$$

and is non-negative if α is selected carefully according to γ . In this study, α is specified as a once continuously differentiable function of γ ,

$$\begin{aligned} \gamma \geq 0.25, & \quad \alpha = 1, \\ \gamma \leq 0, & \quad \alpha = \beta \exp\left(\frac{\gamma}{\beta}\right), \\ 0 < \gamma < 0.25, & \quad \alpha = \beta + \gamma + (40 - 48\beta)\gamma^2 + (128\beta - 112)\gamma^3, \end{aligned} \quad (51)$$

where β is a positive parameter. The values of α and $\tilde{\gamma}$ as functions of γ are shown in figure 3 with $\beta = 10^{-4}$.

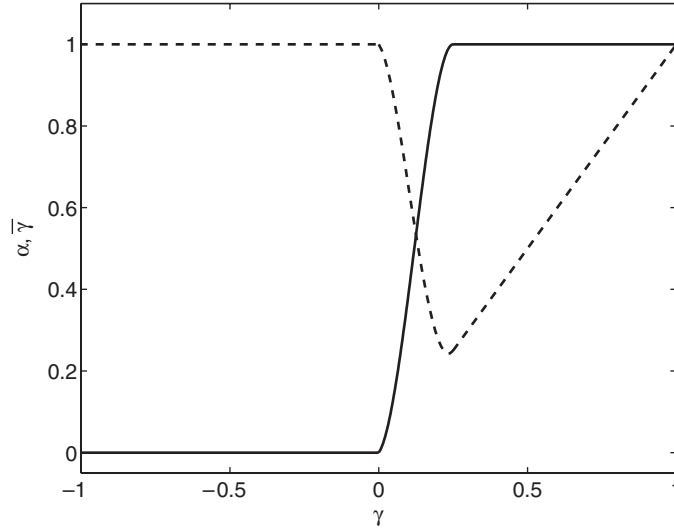


Figure 3. A specification of the blending factor, α (—), and the resulting actual ratio of entropy production rates, $\bar{\gamma}$ (- - -), in CPIM as functions of the entropy production ratio, γ .

6. Rate equation of Lagrange multipliers

We now consider the simplest case of a reactive ideal gas mixture, although the methodology developed is generally applicable to other complex situations. The system is spatially homogeneous, adiabatic and isobaric. The thermodynamic state of the mixture is completely determined by $n_s + 2$ variables, i.e. the species moles, N_i , the enthalpy, H , and the pressure, p . The equation system that describes the time-dependent development of these properties can be written as

$$\dot{H} = \frac{dH}{dt} = 0, \quad (52)$$

$$\dot{p} = \frac{dp}{dt} = 0 \quad (53)$$

and

$$\dot{N} = \frac{dN}{dt} = \mathbf{r}. \quad (54)$$

As mentioned before, only the rate equations for the n_c constraints \mathbf{c} are needed to determine the state of the system in the RCCE method, given H and p . The rate equation for \mathbf{c} equation (24) (for the unmodified RCCE method) is restated here:

$$\dot{\mathbf{c}} = \mathbf{B}^T \dot{N} = \mathbf{B}^T \mathbf{r}. \quad (55)$$

Note that the rate-of-change vector, \mathbf{r} , is now a function of the constrained equilibrium composition, N^{CE} , at given enthalpy H and pressure p .

Given the initial conditions, equations (52), (53) and (55) can be integrated together in a stepwise fashion. Since \mathbf{r} must be evaluated on the CEM, at each step the constrained equilibrium composition must be computed via solving the $n_c + 1$ non-linear equations (18) and (19). For this reason the calculations for small systems, in which the number of species is not very much larger than the number of constraints, may take more CPU time than that required to integrate the full set of rate equations (Keck 1990).

In fact, the RCCE problem can be solved in a totally different way without pursuing the constrained equilibrium composition via solving a complex non-linear system many times. The alternative approach is to integrate the rate equation for the Lagrange multipliers. As discussed in the previous section, for each constraint there is a corresponding Lagrange multiplier, and the constrained equilibrium composition is explicitly determined by λ through equation (21). This approach was first suggested by Keck (1990) and reviewed later by Hamiroune *et al* (1998).

Starting from the non-linear equation system (18), (19) and (20), which determines the CEM, the rate equation of Lagrange multipliers can be derived and written in matrix form:

$$\begin{bmatrix} \mathbf{I} & \mathbf{E}_T & \mathbf{0} \\ \mathbf{F}^T & G_T & G_c \\ \mathbf{0} & 0 & 1 \end{bmatrix} \begin{bmatrix} \dot{\lambda} \\ \dot{T} \\ \dot{|\mathbf{c}|} \end{bmatrix} = \begin{bmatrix} \xi \\ 0 \\ R_c \end{bmatrix}, \quad (56)$$

where \mathbf{I} is an $n_c \times n_c$ identity matrix; \mathbf{E}_T and \mathbf{F}^T are $n_c \times 1$ and $1 \times n_c$ vectors, respectively, G_T and G_c are scalars, and $|\mathbf{c}| \equiv (\mathbf{c}^T \mathbf{c})^{1/2}$ is the two-norm of the constraint vector \mathbf{c} . The procedure for the derivation of equation (56) and the definitions of the variables in the equation are given in appendix B. In particular, the $n_c \times 1$ vector ξ on the right-hand side is a function of θ , with

$$\theta = \frac{1}{\bar{N}} \left(\mathbf{I} - \frac{\mathbf{c}\mathbf{c}^T}{\mathbf{c}^T \mathbf{c}} \right) \mathbf{B}^T \mathbf{r} \quad (57)$$

and the scalar R_c is defined as

$$R_c \equiv \frac{\mathbf{c}^T \mathbf{B}^T \mathbf{r}}{|\mathbf{c}|}. \quad (58)$$

For CPIM, the equations describe the time evolving of λ , T and $|\mathbf{c}|$ are of the same forms as those in equation (56). The differences are

$$\theta = \frac{1}{\bar{N}} \left(\mathbf{I} - \frac{\mathbf{c}\mathbf{c}^T}{\mathbf{c}^T \mathbf{c}} \right) \mathbf{B}^T \tilde{\mathbf{r}} \quad (59)$$

and

$$R_c \equiv \frac{\mathbf{c}^T \mathbf{B}^T \tilde{\mathbf{r}}}{|\mathbf{c}|}, \quad (60)$$

where $\tilde{\mathbf{r}}$ is defined in equation (49).

The RCCE and CPIM can be easily incorporated into the ISAT algorithm through the Lagrange multipliers. The centre-piece of the combined scheme is the linear retrieval process in the n_c -dimensional constraint subspace, which can be expressed as

$$\mathbf{c}^+(\mathbf{c}^\circ + \delta\mathbf{c}) \approx \mathbf{c}^\ell(\mathbf{c}^\circ + \delta\mathbf{c}) \equiv \mathbf{c}^+(\mathbf{c}^\circ) + \mathbf{A}\delta\mathbf{c}, \quad (61)$$

where the superscripts $+$ and \circ refer to the quantities at the initial time and after a time period of Δt , respectively. The $n_c \times n_c$ mapping gradient matrix \mathbf{A} can be written as $\mathbf{A} = \hat{\mathbf{A}}\bar{\mathbf{A}}\check{\mathbf{A}}$ by the chain rule, where $\hat{A}_{jl}(\lambda^+) = \partial c_j^+ / \partial \lambda_l^+$ represents the derivatives of the constraint vector with respect to the Lagrange multipliers and can be calculated using a divided difference scheme or automatic differentiation tools such as Adifor (Bischof *et al* 1992) via equations (18), (19) and (20); the middle term, $\bar{A}_{lm} = \partial \lambda_l^+ / \partial \lambda_m^\circ$, represents the sensitivity of the solution of equation (56) to the initial condition, and can be calculated by the ODE solver (e.g. DDASAC) (Caracotsios and Stewart 1985) while solving the rate equation; and the last term, $\check{A}_{mk} = \partial \lambda_m^\circ / \partial c_k^\circ$, is simply the inverse of $\hat{\mathbf{A}}$ but evaluated at λ° .

7. Test results and discussion

Two combustion systems, i.e. the H_2/air system ($n_s = 9$) and the CH_4/air system (GRI1.2, $n_s = 31$), are chosen to test the CPIM method. For more information about the detailed mechanisms describing the two systems, see Maas and Warnatz (1988) and Smith *et al* (1999), respectively.

The test calculations are made in the idealized plug-flow-reactor (PFR), where a premixed mixture of fuel–air evolves from its initial state eventually to the complete equilibrium state. We refer to this test as the autoignition test case. Each calculation is carried out in the following way: given the initial composition, \mathbf{N} , of the mixture, the initial constraints, \mathbf{c}° , are computed using equation (6). We then solve the non-linear system equation, equation (18), and equation (19) to find out the initial \mathbf{N}^{CE} and the corresponding λ° . The rate equation, equation (56), is integrated over a time period of Δt for λ° . The composition after time Δt is calculated using equation (21). The above process is repeated for many times until the complete equilibrium state is reached. The predicted autoignition delays and the time evolutions of the chemical species are then compared with the exact solutions using detailed mechanisms and the full set of rate equations for all the species. Adiabatic and isobaric conditions are assumed in all calculations.

7.1. H_2/air system

For the H_2/air system, in addition to the time-independent constraints imposed by the conservation of elements, three variable linear constraints are used in the calculations. Among them are the following: the total number of moles, denoted by TM, which is imposed by slow dissociation/recombination reactions; the ‘active valence’ ($\text{AV} = \text{H} + \text{OH} + 2\text{O}$), which is related to the total number of radicals and is imposed by the slow branching reactions; the ‘free oxygen’ ($\text{FO} = \text{O} + \text{OH} + \text{H}_2\text{O}$), which is defined as any oxygen that is not bonded to another oxygen and is imposed by the reactions where the O–O bond is broken. A detailed analysis of these constraints can be found in the literature (e.g. Bishnu *et al* 1997).

The initial major species-specific moles (moles per unit mass) are 0.05, 0.5, 0.15 and 0.3 for H_2O , N_2 , O_2 and H_2 , respectively. For other minor species, their specific moles are set to be a small (chemically insignificant) positive number (i.e. 1.0×10^{-15}), since at the constrained equilibrium state, species compositions must be strictly positive. The initial temperature, T_0 , is 1500 K, and the pressure, p , is 1.0 atm.

Figure 4 shows the calculated temperatures against time using two variable constraints ($n_c = 5$). Among the three RCCE calculations, the combination of TM and AV gives the best estimation of the ignition delay time (which can be defined as the time when temperature rises 10% from the initial temperature), while the combination of AV and FO gives the poorest estimation. However, at the high temperature range, i.e. $T > 2400$ K, the temperature–time curve from the case using AV + FO becomes closer to the exact solution than the other two cases.

Comparisons of the results between the CPIM and the RCCE calculations are very encouraging. In each of the three combinations, the CPIM result shows a greater accuracy (dashed line) than does that of RCCE (dash–dotted line) without exception; in particular, for the case using TM + AV, the result is in excellent agreement with the exact solution throughout the calculation. The comparisons among the three CPIM calculations show that, in the high temperature range ($T > 2400$ K), the temperature–time curves are all very close to the accurate result. However, in predicting the ignition delay, the errors in the cases using TM + FO and AV + FO are still high, with the latter giving the worst result, which is consistent with the

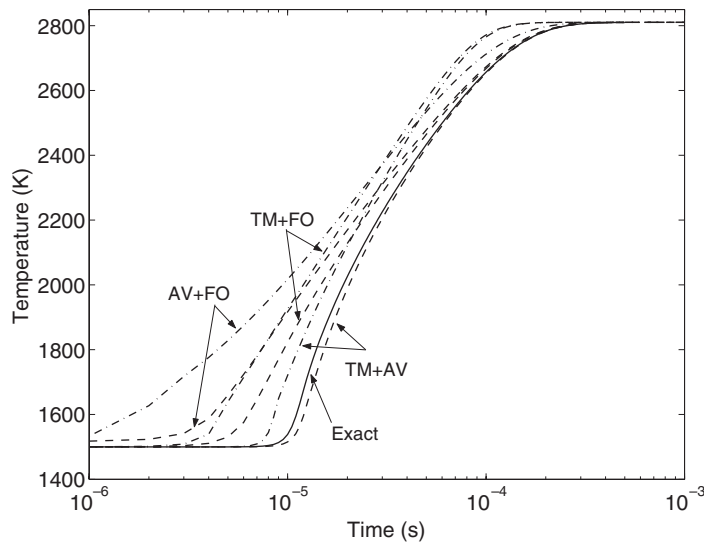


Figure 4. Temperature as a function of time using two time-dependent constraints. —, exact solution; — · —, RCCE; - - -, CPIM.

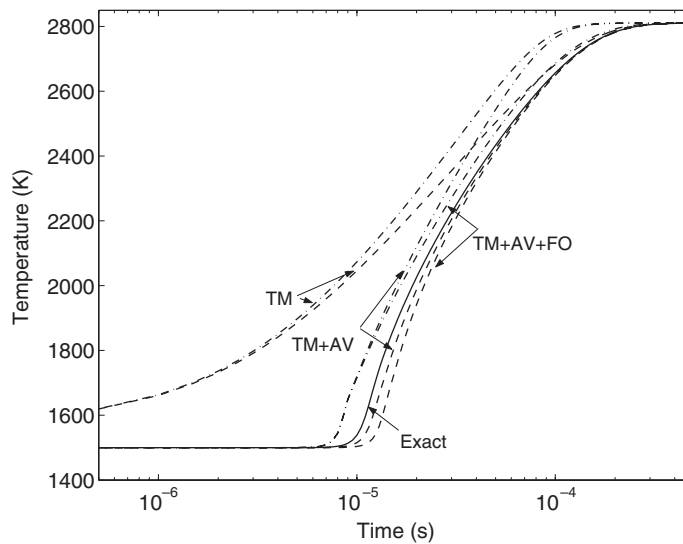


Figure 5. Effects of the number of constraints on RCCE/CPIM calculations. —, exact solution; — · —, RCCE; - - -, CPIM.

observation from the three RCCE calculations. Nevertheless, the results plotted in figure 4 show that the CPIM calculations are less dependent on the choices of the constraint subspace than the RCCE calculations.

The effects of the number of constraints are shown in figure 5. Starting from the calculation using TM, we add the other constraints one at a time in the order AV followed by FO. For RCCE, using TM only is not able to predict the temperature–time curve correctly. The addition of AV improves the result dramatically in the lower temperature range, which results in a much better prediction of the ignition delay time. The benefit from FO is mainly seen in the higher

Table 1. Constraints (in addition to the four element constraints) considered in the RCCE/CPIM calculations for the CH₄/air system.

Case 1 ($n_c = 16$)	TM, AV, CO ₂ , H ₂ O, CH ₄ , O ₂ , CO, CH ₃ , H ₂ , C ₂ H ₂ , C ₂ H ₄ , C ₂ H ₆
Case 2 ($n_c = 16$)	TM, AV, CO ₂ , H ₂ O, CH ₄ , O ₂ , CO, CH ₃ , H ₂ , HO ₂ , H ₂ O ₂ , C ₂ H ₂
Case 3 ($n_c = 18$)	TM, AV, CO ₂ , H ₂ O, CH ₄ , O ₂ , CO, CH ₃ , H ₂ , C ₂ H ₂ , C ₂ H ₄ , C ₂ H ₆ , HO ₂ , H ₂ O ₂
Case 4 ($n_c = 20$)	TM, CO ₂ , H ₂ O, CH ₄ , O ₂ , CO, CH ₃ , H ₂ , C ₂ H ₂ , C ₂ H ₄ , C ₂ H ₆ , HO ₂ , H ₂ O ₂ , H, OH, O

temperature range ($T > 1800$ K). For CPIM, the improvement is observed in the higher temperature range ($T > 2000$ K) for the case using TM only. The case using TM and AV is still the best one, while the case using all three variable constraints predicts ignition delay time slightly longer, which implies that the addition of FO may have some negative impact on the CPIM assumption.

7.2. CH₄/air system

In this study, the RCCE and the CPIM calculations are carried out for a stoichiometric mixture of CH₄ and air at an initial temperature of $T_0 = 1500$ K and pressure of $p = 1$ atm. The initial specific moles of major species are 0.715, 0.19, 0.095, 0.03 and 0.02 for N₂, O₂, CH₄, CO₂ and H₂O, respectively. All other species have the same specific moles of 1.0×10^{-15} initially.

The CH₄/air system is much more complex than the H₂/air system. In addition to the element constraints and the linear constraints TM and AV defined for the H₂/air system, constraints are imposed on individual species-specific moles. The selection of these individual species constraints is based mainly on experience, and essentially all major species are included. In this respect RCCE is similar to QSSA and inferior to ILDM where the slow subspace is determined automatically and is independent of the choice of the reduced variables. A more general methodology to find the optimal constraint subspace in RCCE is currently under investigation. Four cases with different sets of constraints are summarized in table 1.

The calculation results for case 1 are shown in figure 6, where the temperature and some of the species mole fractions are plotted as functions of time. It can be seen that the CPIM results are much more accurate than the RCCE results. For temperature and major species such as CO₂, CH₄ and CO, the CPIM results are in near-perfect agreement with the exact solution. For the three most active radicals, H, OH and O, which are controlled by the constraint AV, the CPIM results are also very accurate during the ignition and recombination periods, whereas in the initiation stage, the concentrations of these species first follow the RCCE results (due to the infeasibility of CPIM and the blending with the RCCE results) and then recover to the values of the exact solution. It can be seen that the mole fraction of radical O in figure 6(h) is far from the exact value in the entire induction period and in the early stage of ignition. However, the time and the magnitude of the peak mole fraction of O are accurately predicted by CPIM.

Another observation is that the set of constraints in case 1 does not function correctly for the important radical HO₂ and species H₂O₂, which can be seen in figure 6(i) and (j), where the concentration of HO₂ calculated by CPIM is too low in the induction and ignition stages, whereas the concentration of H₂O₂ is too high.

Case 2 aims to predict the mole fractions of HO₂ and H₂O₂ correctly: we replace the constrained species C₂H₄ and C₂H₆ in case 1 by HO₂ and H₂O₂ and keep the dimensionality of the constraint subspace the same. The results are presented in figure 7.

The interesting finding is that the accuracy of the RCCE calculation is improved dramatically in terms of the ignition delay time, the temperature and the mole fractions of major species. The predictions using CPIM are still better than those using RCCE overall, except for the radical OH in the induction period (figure 7(g)).

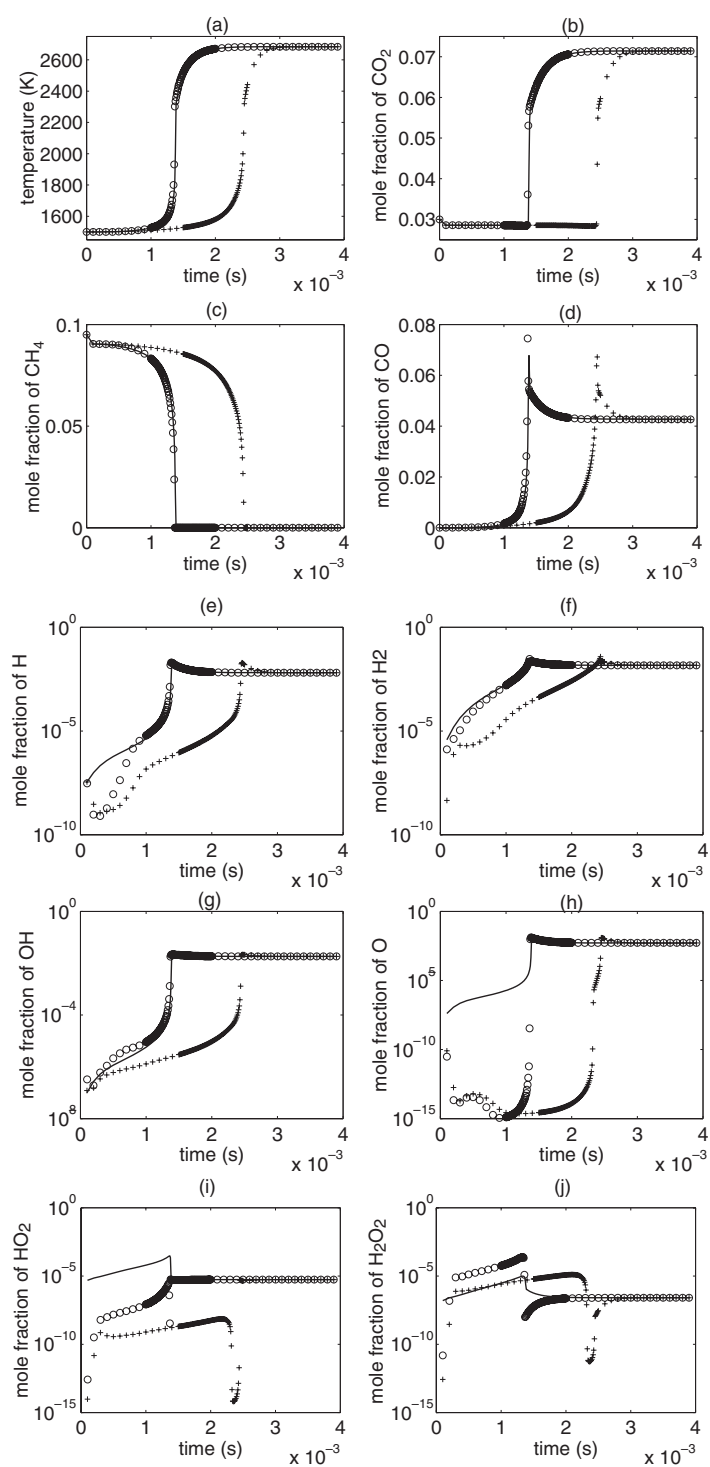


Figure 6. Case 1: temperature and species mole fractions as functions of time for CH_4/air autoignition. —, exact solution; \circ , CPIM; +, RCCE.

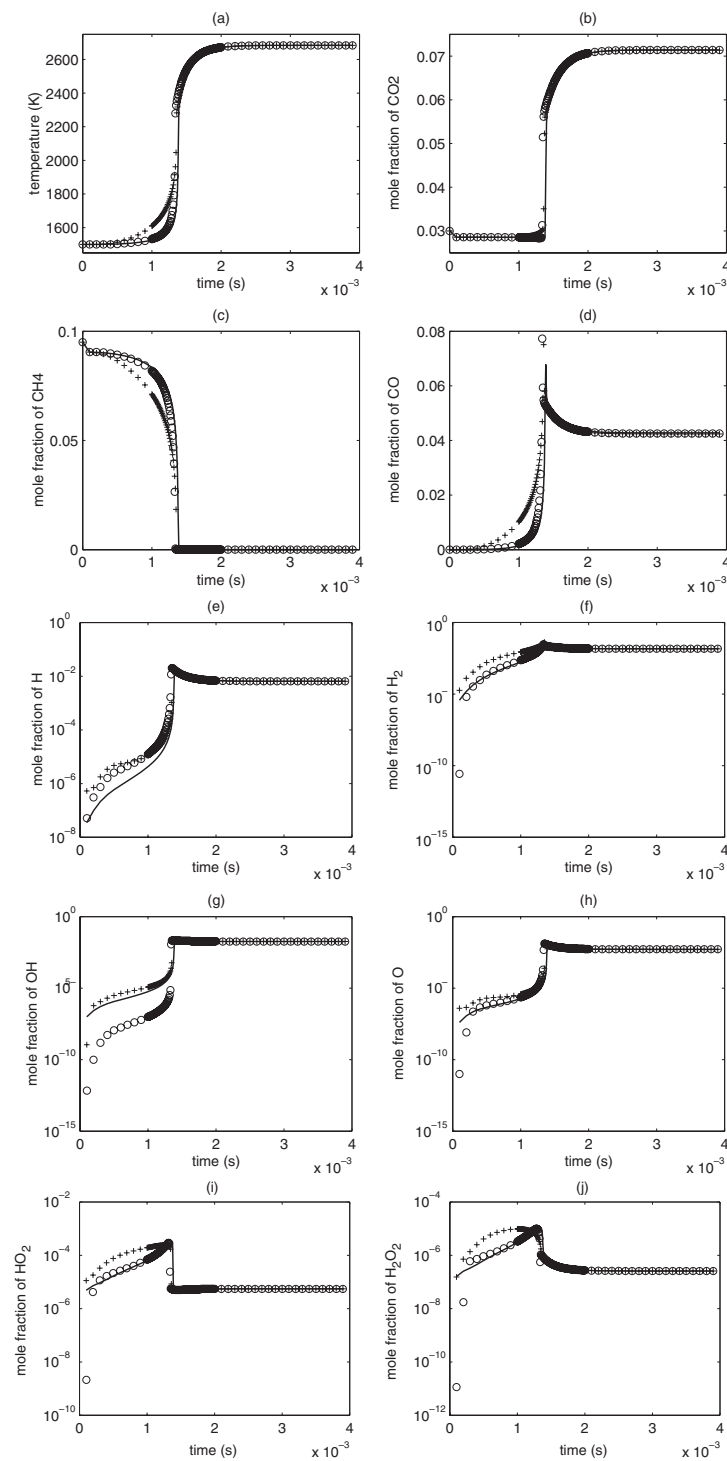


Figure 7. Case 2: temperature and species mole fractions as functions of time for CH_4/air autoignition. —, exact solution; \circ , CPIM; +, RCCE.

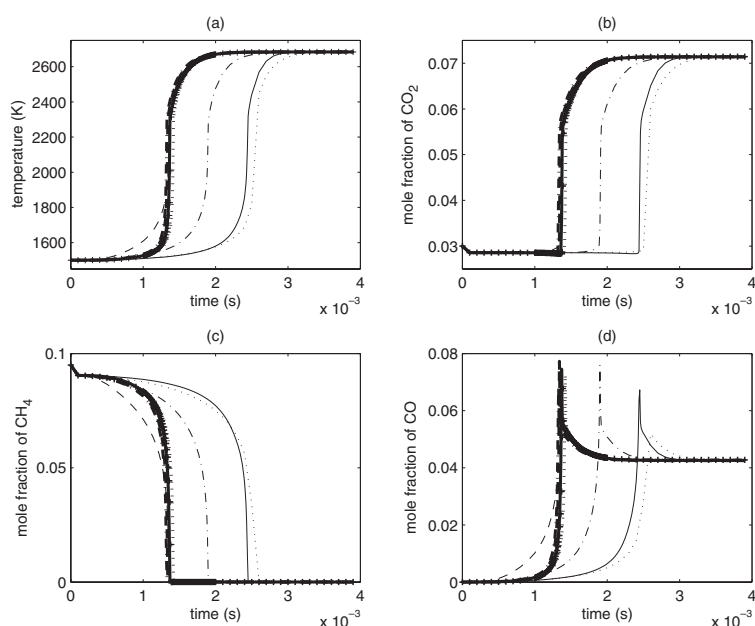


Figure 8. Comparisons of temperature and species mole fractions calculated using RCCE and CPIM. Symbol, exact solution; bold line, CPIM; fine line, RCCE; solid line, case 1; dashed line, case 2; dash-dotted line, case 3; dotted line, case 4.

For CPIM, compared with the case 1 results, the calculated ignition delay time is slightly shorter. The most prominent improvements are for the radicals O and HO₂, and for the species H₂O₂, which are shown in figures 7(h)–(j). Similar improvements are also found in the results using RCCE. The reason for this has not yet been fully established, but a strong possibility is that in case 1, the reaction $\text{HO}_2 + \text{CH}_2\text{O} \rightleftharpoons \text{HCO} + \text{H}_2\text{O}_2$ is assumed to be in partial equilibrium, whereas in case 2 it is not because of the constraints on HO₂ and H₂O₂.

Figure 8 shows the evolutions of temperature and mole fractions of major species calculated in all four cases. It may be noted that for all four cases, the CPIM results predict the ignition delay time accurately and the shapes of the time evolutions of temperature and major species are reproduced nearly perfectly. The differences among the four cases for these quantities are negligible. In contrast, the RCCE calculations in these cases are not able to compete with CPIM in terms of accuracy. This suggests that the CPIM is a good approximation to the slow attracting manifold and the CPIM is not very sensitive to the choice of constraint subspaces, whereas for RCCE, the correlation is strong.

The main differences among these cases are highlighted in figure 9. It may be seen that the mole fractions of HO₂ and H₂O₂ are not well predicted in case 1, while they are accurately predicted in the other three cases where they belong to the constraint subspaces.

8. Conclusions

Using the concept of the CEM, a hidden assumption in RCCE is exposed, which corresponds to an orthogonal projection of the rate-of-change of species composition due to reaction onto the manifold. An alternative projection aiming at improving the dimension-reduction accuracy is obtained, which is linked to the local Jacobian by assuming that, near the CEM, there is a CPIM.

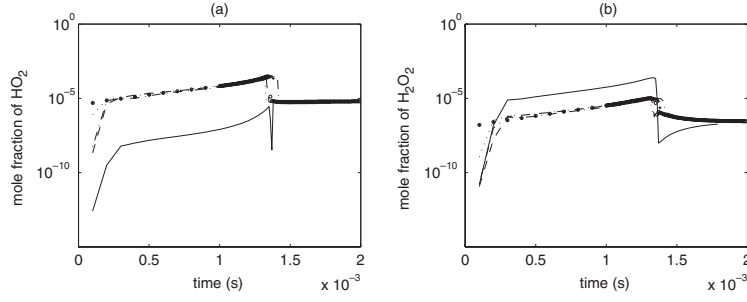


Figure 9. Comparisons of minor species mole fractions calculated using CPIM. Symbols, exact solution; solid line, case 1; dashed line, case 2; dotted line, case 3; dash-dotted line, case 4.

The CPIM method shows great promise in improving the dimension-reduction accuracy. In the autoignition test calculations, with an initial temperature $T_0 = 1500$ K, the CPIM results are in excellent agreement with the exact solution using the detailed mechanism and are much better than the corresponding RCCE calculations, while the dimension reductions are from 9 to 5 and from 31 to 16, for the two reaction systems, respectively. The CPIM method also shows less dependence upon the choice of constraint subspace. In the autoignition calculations for the CH_4/air system, the CPIM calculations with four different sets of constraints achieve the same level of accuracy. In contrast, the performance of RCCE is very sensitive to the choice of constraints.

Acknowledgment

This work is supported by Air Force Office of Scientific Research grant F-49620-03-1-0015.

Appendix A. The tangent subspace of the CEM

In the CPIM method, we assume that the constrained equilibrium composition, N^{CE} , is a differentiable function of the constraint vector \mathbf{c} . As a consequence, the derivatives of the constrained equilibrium composition vector with respect to the constraint vector, denoted by $\hat{T}_{ij} \equiv \partial N_i / \partial c_j$, must be a unique function of \mathbf{c} , given H and p . In this appendix, an analytical expression of the matrix $\hat{\mathbf{T}}$ with its entries being \hat{T}_{ij} is derived for fixed H and p . The column vectors of $\hat{\mathbf{T}}$ span the tangent subspace of the CEM, and $\hat{\mathbf{T}}$ is used in the construction of the CPIM method.

On the CEM, the number of moles of species i can be written as

$$N_i = \bar{N} \exp(-\tilde{g}_i + B_{il}\lambda_l), \quad (\text{A.1})$$

where \bar{N} is the total number of moles of the mixture; $\tilde{\mathbf{g}}$ is the normalized standard Gibbs function; \mathbf{B} is the constraint matrix; and $\boldsymbol{\lambda}$ is the vector of Lagrangian multipliers. Differentiating equation (A.1) with respect to c_j , we obtain

$$\frac{\partial N_i}{\partial c_j} = N_i \frac{\partial \ln \bar{N}}{\partial c_j} - N_i \frac{\partial \tilde{g}_{(i)}}{\partial c_j} + N_i B_{(i)l} \frac{\partial \lambda_l}{\partial c_j}, \quad (\text{A.2})$$

where the subscripts in brackets are excluded from the summation convention. Multiplying equation (A.2) by B_{ki} , we obtain

$$\delta_{kj} = c_k \frac{\partial \ln \bar{N}}{\partial c_j} - B_{ki} N_i \frac{\partial \tilde{g}_{(i)}}{\partial c_j} + \tilde{D}_{kl} \frac{\partial \lambda_l}{\partial c_j}, \quad (\text{A.3})$$

where

$$\tilde{D}_{kl} \equiv \bar{N} B_{ki} X_{im} B_{ml} \quad (\text{A.4})$$

and \mathbf{X} is an $n_s \times n_s$ diagonal matrix, with its diagonal entries being species mole fractions in the constrained equilibrium state:

$$\mathbf{X} \equiv \text{diag}(X_1, X_2, \dots, X_{n_s}). \quad (\text{A.5})$$

Equation (A.3) can be solved for $\partial\lambda_l/\partial c_j$:

$$\frac{\partial\lambda_l}{\partial c_j} = \tilde{D}_{lj}^{-1} - \tilde{D}_{kl}^{-1} c_k \frac{\partial \ln \bar{N}}{\partial c_j} + \tilde{D}_{kl}^{-1} B_{ki} N_i \frac{\partial \tilde{g}_i}{\partial c_j}. \quad (\text{A.6})$$

Summing equation (A.2) over subscript i for $i = 1, \dots, n_s$, we obtain

$$\sum_i \frac{\partial N_i}{\partial c_j} = \frac{\partial \bar{N}}{\partial c_j} = \frac{\partial \bar{N}}{\partial c_j} - N_i \frac{\partial \tilde{g}_i}{\partial c_j} + c_l \frac{\partial \lambda_l}{\partial c_j} \quad (\text{A.7})$$

and

$$c_l \frac{\partial \lambda_l}{\partial c_j} = N_i \frac{\partial \tilde{g}_i}{\partial c_j}. \quad (\text{A.8})$$

Let $L_{lj} \equiv \partial\lambda_l/\partial c_j$, $\mu_j \equiv \partial \ln \bar{N}/\partial c_j$ and $\tilde{G}_{ij} \equiv \partial \tilde{g}_i/\partial c_j$; then equations (A.6) and (A.8) can be written in matrix form:

$$\begin{aligned} \mathbf{L} &= \tilde{\mathbf{D}}^{-1} - \tilde{\mathbf{D}}^{-1} \mathbf{c} \boldsymbol{\mu} + \bar{N} \tilde{\mathbf{D}}^{-1} \mathbf{B}^T \mathbf{X} \tilde{\mathbf{G}}, \\ \mathbf{c}^T \mathbf{L} &= N^T \tilde{\mathbf{G}}. \end{aligned} \quad (\text{A.9})$$

Solving equation (A.9) for \mathbf{L} and $\boldsymbol{\mu}$, we obtain

$$\mathbf{L} = \tilde{\mathbf{D}}^{-1} - \frac{\tilde{\mathbf{D}}^{-1} \mathbf{c} \mathbf{c}^T \tilde{\mathbf{D}}^{-1}}{\mathbf{c}^T \tilde{\mathbf{D}}^{-1} \mathbf{c}} + \left(\frac{\tilde{\mathbf{D}}^{-1} \mathbf{c} N^T - \bar{N} \tilde{\mathbf{D}}^{-1} \mathbf{c} \mathbf{c}^T \tilde{\mathbf{D}}^{-1} \mathbf{B}^T \mathbf{X}}{\mathbf{c}^T \tilde{\mathbf{D}}^{-1} \mathbf{c}} + \bar{N} \tilde{\mathbf{D}}^{-1} \mathbf{B}^T \mathbf{X} \right) \tilde{\mathbf{G}} \quad (\text{A.10})$$

and

$$\boldsymbol{\mu} = \frac{\mathbf{c}^T \tilde{\mathbf{D}}^{-1}}{\mathbf{c}^T \tilde{\mathbf{D}}^{-1} \mathbf{c}} + \left(\frac{\bar{N} \mathbf{c}^T \tilde{\mathbf{D}}^{-1} \mathbf{B}^T \mathbf{X} - N^T}{\mathbf{c}^T \tilde{\mathbf{D}}^{-1} \mathbf{c}} \right) \tilde{\mathbf{G}}. \quad (\text{A.11})$$

Substituting equation (A.10) and equation (A.11) into equation (A.2), we obtain

$$\begin{aligned} \hat{\mathbf{T}} &= N \boldsymbol{\mu} - \bar{N} \mathbf{X} \tilde{\mathbf{G}} + \bar{N} \mathbf{X} \mathbf{B} \mathbf{L} = \bar{N} \mathbf{X} \mathbf{B} \tilde{\mathbf{D}}^{-1} + \frac{N \mathbf{c}^T \tilde{\mathbf{D}}^{-1} - \bar{N} \mathbf{X} \mathbf{B} \tilde{\mathbf{D}}^{-1} \mathbf{c} \mathbf{c}^T \tilde{\mathbf{D}}^{-1}}{\mathbf{c}^T \tilde{\mathbf{D}}^{-1} \mathbf{c}} \\ &\quad + \left(\frac{\bar{N} N \mathbf{c}^T \tilde{\mathbf{D}}^{-1} \mathbf{B}^T \mathbf{X} - N N^T + \bar{N} \mathbf{X} \mathbf{B} \tilde{\mathbf{D}}^{-1} \mathbf{c} N^T}{\mathbf{c}^T \tilde{\mathbf{D}}^{-1} \mathbf{c}} \right) \tilde{\mathbf{G}} - \frac{\bar{N}^2 \mathbf{X} \mathbf{B} \tilde{\mathbf{D}}^{-1} \mathbf{c} \mathbf{c}^T \tilde{\mathbf{D}}^{-1} \mathbf{B}^T \mathbf{X}}{\mathbf{c}^T \tilde{\mathbf{D}}^{-1} \mathbf{c}} \tilde{\mathbf{G}} \\ &\quad + \left(\bar{N}^2 \mathbf{X} \mathbf{B} \tilde{\mathbf{D}}^{-1} \mathbf{B}^T \mathbf{X} - \bar{N} \mathbf{X} \right) \tilde{\mathbf{G}}. \end{aligned} \quad (\text{A.12})$$

To simplify the notation, we write the above equation as

$$\hat{\mathbf{T}} = \tilde{\mathbf{A}} + \tilde{\mathbf{F}} \tilde{\mathbf{G}}, \quad (\text{A.13})$$

where the matrix $\tilde{\mathbf{G}}$ can be related to $\hat{\mathbf{T}}$ by the chain rule (with fixed H and p),

$$\frac{\partial \tilde{g}_i}{\partial c_j} = \frac{\partial \tilde{g}_i}{\partial T} \frac{\partial T}{\partial N_k} \frac{\partial N_k}{\partial c_j} = -\frac{h_i}{\mathcal{R}T^2} \frac{\partial T}{\partial N_k} \frac{\partial N_k}{\partial c_j} \quad (\text{A.14})$$

or in matrix form,

$$\tilde{\mathbf{G}} = \tilde{\mathbf{H}} \hat{\mathbf{T}} \quad (\text{A.15})$$

with

$$\tilde{H}_{ik} \equiv -\frac{h_i}{\mathcal{R}T^2} \frac{\partial T}{\partial N_k}. \quad (\text{A.16})$$

The term $\partial T/\partial N_k$ can be calculated using the finite difference method or automatic differentiation tools, given H , p and the mixture composition N .

Substituting equation (A.15) into equation (A.13), we obtain

$$(\mathbf{I} - \tilde{\mathbf{F}}\tilde{\mathbf{H}})\hat{\mathbf{T}} = \tilde{\mathbf{A}}. \quad (\text{A.17})$$

The matrix $\hat{\mathbf{T}}$ can be calculated by solving the above linear equation system, while we argue that the existence and uniqueness of the solution are guaranteed by the assumption of the differentiable CEM.

It can be shown that matrix $\tilde{\mathbf{D}}$ defined in equation (A.4) is symmetric positive definite (Tang 2003), given the fact that, on the CEM, species mole fractions are strictly positive. However, when calculations are performed on a computer (i.e. floating point numbers are used), the matrix can be essentially singular with respect to the machine precision, and so the occurrences of $\tilde{\mathbf{D}}^{-1}$ in equation (A.9) and elsewhere in this section are problematic. To overcome this problem, a well-conditioned pseudo-inverse of $\tilde{\mathbf{D}}$, which is constructed in the same way as the pseudo-inverse of \mathbf{K} in section 5 with $\zeta = 1.0 \times 10^{-8}$, is used in place of $\tilde{\mathbf{D}}^{-1}$.

Appendix B. Derivation of the rate equation of Lagrange multipliers

In this appendix, we derive the rate equation of Lagrange multipliers as well as two additional rate equations under the condition of fixed H and p . In the RCCE method, this set of ordinary differential equations can be integrated to describe the time evolutions of a reactive ideal gas mixture.

We start from the following non-linear equation system that determines the CEM:

$$\tilde{N}\mathbf{B}^T\mathbf{X} = \mathbf{B}^T\mathbf{N} = \mathbf{c} \quad (\text{B.1})$$

and

$$\sum_{i=1}^{n_s} X_i = 1, \quad (\text{B.2})$$

where

$$X_i = \exp(-\tilde{g}_i + B_{ij}\lambda_j). \quad (\text{B.3})$$

Adiabatic and isobaric conditions are assumed. Equation (B.1) can also be written as

$$\tilde{N}\mathbf{v} = \mathbf{c}, \quad (\text{B.4})$$

where

$$\mathbf{v} \equiv \mathbf{B}^T\mathbf{X}. \quad (\text{B.5})$$

It follows that

$$\tilde{N} = \frac{|\mathbf{c}|}{|\mathbf{v}|} \quad (\text{B.6})$$

with $|\mathbf{c}| = (\mathbf{c}^T\mathbf{c})^{1/2}$ and $|\mathbf{v}| = (\mathbf{v}^T\mathbf{v})^{1/2}$, and the constraint direction is defined by the unit vector

$$\bar{\mathbf{c}} \equiv \frac{\mathbf{c}}{|\mathbf{c}|} = \frac{\mathbf{v}}{|\mathbf{v}|}. \quad (\text{B.7})$$

Differentiating equation (B.7) with respect to time t , we obtain

$$\frac{d}{dt} \left(\frac{\mathbf{v}}{|\mathbf{v}|} \right) = \left(\mathbf{I} - \frac{\mathbf{v}\mathbf{v}^T}{\mathbf{v}^T\mathbf{v}} \right) \frac{\dot{\mathbf{v}}}{|\mathbf{v}|} = \frac{d}{dt} \left(\frac{\mathbf{c}}{|\mathbf{c}|} \right) \quad (\text{B.8})$$

and

$$\left(\mathbf{I} - \frac{\mathbf{v}\mathbf{v}^T}{\mathbf{v}^T\mathbf{v}} \right) \dot{\mathbf{v}} = \boldsymbol{\theta} \equiv |\mathbf{v}| \frac{d}{dt} \left(\frac{\mathbf{c}}{|\mathbf{c}|} \right) = \frac{|\mathbf{v}|}{|\mathbf{c}|} \left(\mathbf{I} - \frac{\mathbf{c}\mathbf{c}^T}{\mathbf{c}^T\mathbf{c}} \right) \dot{\mathbf{c}} \quad (\text{B.9})$$

$$= \frac{1}{\bar{N}} \left(\mathbf{I} - \frac{\mathbf{c}\mathbf{c}^T}{\mathbf{c}^T\mathbf{c}} \right) \mathbf{B}^T \mathbf{r}. \quad (\text{B.10})$$

Note that $\mathbf{v}^T \boldsymbol{\theta} = 0$.

For constant p and H , differentiating equations (B.3) and (B.5) yields

$$\dot{v}_j = B_{ji} \dot{X}_i = B_{ji} X_i B_{(i)k} \dot{\lambda}_k - B_{ji} X_i \dot{\tilde{g}}_{(i)}, \quad (\text{B.11})$$

where the subscripts in brackets are excluded from the summation convention. The second term in the right-hand side of equation (B.11) can be related to the rate-of-change of temperature by the chain rule:

$$\dot{\tilde{g}}_i = \frac{d\tilde{g}_i}{dT} \dot{T}. \quad (\text{B.12})$$

Recall the definition of \tilde{g}_i from equation (11):

$$\tilde{g}_i = \frac{h_i}{\mathcal{R}T} - \frac{s_i^0}{\mathcal{R}} + \ln \left(\frac{p}{p_{\text{atm}}} \right) = \frac{1}{\mathcal{R}T} g_i^0 + \ln \left(\frac{p}{p_{\text{atm}}} \right), \quad (\text{B.13})$$

where $g_i^0 \equiv h_i - Ts_i^0$ is the standard Gibbs function of species i . It follows that

$$\frac{d\tilde{g}_i}{dT} = -\frac{h_i}{\mathcal{R}T^2}. \quad (\text{B.14})$$

Thus, equation (B.11) can be rewritten as

$$\dot{v}_j = B_{ji} X_i B_{(i)k} \dot{\lambda}_k + B_{ji} X_i h_{(i)} \frac{\dot{T}}{\mathcal{R}T^2}. \quad (\text{B.15})$$

Substituting equation (B.15) into equation (B.9), we obtain

$$\left(\mathbf{I} - \frac{\mathbf{v}\mathbf{v}^T}{\mathbf{v}^T\mathbf{v}} \right) \mathbf{M} \dot{\boldsymbol{\lambda}} + \left(\mathbf{I} - \frac{\mathbf{v}\mathbf{v}^T}{\mathbf{v}^T\mathbf{v}} \right) \mathbf{B}^T \mathbf{X} \mathbf{h} \frac{\dot{T}}{\mathcal{R}T^2} = \boldsymbol{\theta}, \quad (\text{B.16})$$

where \mathbf{M} is an $n_c \times n_c$ matrix defined as

$$\mathbf{M} \equiv \mathbf{B}^T \mathbf{X} \mathbf{B} = \frac{1}{\bar{N}} \tilde{\mathbf{D}}, \quad (\text{B.17})$$

where $\tilde{\mathbf{D}}$ is defined in equation (A.4). The treatment of ill-conditioned \mathbf{M} is the same as that of $\tilde{\mathbf{D}}$ discussed in appendix A.

Differentiating equation (B.2) with respect to time and using equation (B.3), we obtain

$$\sum_{i=1}^{n_s} \dot{X}_i = 0 = X_i B_{ij} \dot{\lambda}_j + X_i h_i \frac{\dot{T}}{\mathcal{R}T^2} \quad (\text{B.18})$$

or equivalently

$$\mathbf{v}^T \dot{\boldsymbol{\lambda}} + \mathbf{X}^T \mathbf{h} \frac{\dot{T}}{\mathcal{R}T^2} = 0. \quad (\text{B.19})$$

Equations (B.16) and (B.19) can be reorganized as

$$\left(\mathbf{I} - \frac{\mathbf{v}\mathbf{v}^T}{\mathbf{v}^T\mathbf{v}}\right)\mathbf{M}\dot{\boldsymbol{\lambda}} = \boldsymbol{\theta} - \left(\mathbf{I} - \frac{\mathbf{v}\mathbf{v}^T}{\mathbf{v}^T\mathbf{v}}\right)\mathbf{B}^T\mathbf{X}\mathbf{h}\frac{\dot{T}}{\mathcal{R}T^2} \quad (\text{B.20})$$

and

$$\mathbf{v}^T\dot{\boldsymbol{\lambda}} = -\mathbf{X}^T\mathbf{h}\frac{\dot{T}}{\mathcal{R}T^2}, \quad (\text{B.21})$$

which $\dot{\boldsymbol{\lambda}}$ must satisfy for given \dot{T} . The solution of equation (B.20) is of the form

$$\dot{\boldsymbol{\lambda}} = \mathbf{M}^{-1}\boldsymbol{\theta} + \alpha\mathbf{M}^{-1}\mathbf{v} - \mathbf{M}^{-1}\mathbf{B}^T\mathbf{X}\mathbf{h}\frac{\dot{T}}{\mathcal{R}T^2}, \quad (\text{B.22})$$

where α is an undetermined scalar. Then equation (B.21) yields

$$\mathbf{v}^T\mathbf{M}^{-1}\boldsymbol{\theta} + \alpha\mathbf{v}^T\mathbf{M}^{-1}\mathbf{v} - \mathbf{v}^T\mathbf{M}^{-1}\mathbf{B}^T\mathbf{X}\mathbf{h}\frac{\dot{T}}{\mathcal{R}T^2} = -\mathbf{X}^T\mathbf{h}\frac{\dot{T}}{\mathcal{R}T^2}$$

and

$$\alpha = \frac{1}{\mathbf{v}^T\mathbf{M}^{-1}\mathbf{v}} \left[-\mathbf{v}^T\mathbf{M}^{-1}\boldsymbol{\theta} + \frac{\dot{T}}{\mathcal{R}T^2} (\mathbf{v}^T\mathbf{M}^{-1}\mathbf{B}^T\mathbf{X}\mathbf{h} - \mathbf{X}^T\mathbf{h}) \right]. \quad (\text{B.23})$$

Substituting equation (B.23) into equation (B.22) and defining

$$\boldsymbol{\gamma} \equiv \frac{\mathbf{B}^T\mathbf{X}\mathbf{h}}{\mathcal{R}T}, \quad (\text{B.24})$$

$$\mathbf{Q} \equiv \mathbf{M}^{-1} - \frac{\mathbf{M}^{-1}\mathbf{v}\mathbf{v}^T\mathbf{M}^{-1}}{\mathbf{v}^T\mathbf{M}^{-1}\mathbf{v}}, \quad (\text{B.25})$$

$$\hat{\mathbf{v}} \equiv \frac{\mathbf{M}^{-1}\mathbf{v}}{\mathbf{v}^T\mathbf{M}^{-1}\mathbf{v}}, \quad (\text{B.26})$$

$$\bar{\mathbf{h}} \equiv \mathbf{X}^T\mathbf{h}, \quad (\text{B.27})$$

we obtain n_c differential equations for $n_c + 2$ unknowns $\boldsymbol{\lambda}$, \bar{N} and T :

$$\dot{\boldsymbol{\lambda}} + \left(\mathbf{Q}\boldsymbol{\gamma} + \frac{\bar{\mathbf{h}}}{\mathcal{R}T}\hat{\mathbf{v}}\right)\frac{\dot{T}}{T} = \mathbf{Q}\boldsymbol{\theta}. \quad (\text{B.28})$$

An additional differential equation can be obtained by relating $|\mathbf{c}|$ with the rate-of-change vector \mathbf{r} . The equation reads

$$|\dot{\mathbf{c}}| = \frac{\mathbf{c}^T}{|\mathbf{c}|}\dot{\mathbf{c}} = \frac{\mathbf{c}^T}{|\mathbf{c}|}\mathbf{B}^T\mathbf{r}. \quad (\text{B.29})$$

The last differential equation can be derived from the expression for the enthalpy:

$$H = \bar{N}X_i h_i. \quad (\text{B.30})$$

Differentiating equation (B.30) gives the following equation:

$$\dot{H} = \dot{\bar{N}}X_i h_i + \bar{N}\dot{X}_i h_i + \bar{N}\bar{C}_p\dot{T} = 0, \quad (\text{B.31})$$

where $\bar{C}_p \equiv X_i\partial h_i/\partial T = X_i C_{pi}$ is the mean specific heat of the mixture and C_{pi} is the specific heat of species i .

From equation (B.6), we have

$$\dot{\bar{N}} = \left(\frac{|\dot{\mathbf{c}}|}{|\mathbf{v}|}\right) = \frac{|\dot{\mathbf{c}}|}{|\mathbf{v}|} - \bar{N}\frac{\mathbf{v}^T}{\mathbf{v}^T\mathbf{v}}\dot{\mathbf{v}}, \quad (\text{B.32})$$

where $|\dot{c}|$ and \dot{v} are given in equation (B.29) and (B.15), respectively. Differentiating equation (B.3) gives

$$\dot{X} = \mathbf{X}\mathbf{B}\dot{\lambda} + \mathbf{X}\mathbf{h} \frac{\dot{T}}{\mathcal{R}T^2}. \quad (\text{B.33})$$

Substituting equations (B.32), (B.33) into equation (B.31), we obtain

$$0 = \left(\gamma^T - \frac{\bar{h}}{\mathcal{R}T} \frac{\mathbf{v}^T \mathbf{M}}{\mathbf{v}^T \mathbf{v}} \right) \dot{\lambda} + \left(\frac{\bar{C}_p}{\mathcal{R}} + \frac{\mathbf{h}^T \mathbf{X}\mathbf{h}}{\mathcal{R}^2 T^2} - \frac{\bar{h}}{\mathcal{R}T} \frac{\mathbf{v}^T \gamma}{\mathbf{v}^T \mathbf{v}} \right) \frac{\dot{T}}{T} + \frac{\bar{h}}{\bar{N}\mathcal{R}T} \frac{|\dot{c}|}{|\mathbf{v}|}. \quad (\text{B.34})$$

To conclude, for fixed H and p , equations (B.28), (B.29) and (B.34) represent $n_c + 2$ linear first-order differential equations that can be integrated to solve the RCCE problem, given the initial conditions. The equations can be written in the form

$$\begin{bmatrix} \mathbf{I} & \mathbf{E}_T & \mathbf{0} \\ \mathbf{F}^T & G_T & G_c \\ \mathbf{0} & 0 & 1 \end{bmatrix} \begin{bmatrix} \dot{\lambda} \\ \dot{T} \\ |\dot{c}| \end{bmatrix} = \begin{bmatrix} \boldsymbol{\xi} \\ 0 \\ R_c \end{bmatrix}, \quad (\text{B.35})$$

where \mathbf{I} is an $n_c \times n_c$ identity matrix;

$$\mathbf{E}_T = \frac{1}{T} \left(\mathbf{Q}\gamma + \frac{\bar{h}}{\mathcal{R}T} \dot{\mathbf{v}} \right)$$

and

$$\mathbf{F}^T = \gamma^T - \frac{\bar{h}}{\mathcal{R}T} \frac{\mathbf{v}^T \mathbf{M}}{\mathbf{v}^T \mathbf{v}},$$

are $n_c \times 1$ and $1 \times n_c$ vectors, respectively; G_T and G_c are scalars evaluated as

$$G_T = \left(\frac{\bar{C}_p}{\mathcal{R}} + \frac{\mathbf{h}^T \mathbf{X}\mathbf{h}}{\mathcal{R}^2 T^2} - \frac{\bar{h}}{\mathcal{R}T} \frac{\mathbf{v}^T \gamma}{\mathbf{v}^T \mathbf{v}} \right) \frac{1}{T}$$

and

$$G_c = \frac{\bar{h}}{\bar{N}\mathcal{R}T|\mathbf{v}|}.$$

On the right-hand side, $\boldsymbol{\xi}$ is an $n_c \times 1$ vector,

$$\boldsymbol{\xi} = \mathbf{Q}\boldsymbol{\theta} = \frac{1}{\bar{N}} \mathbf{Q} \left(\mathbf{I} - \frac{\mathbf{c}\mathbf{c}^T}{\mathbf{c}^T \mathbf{c}} \right) \mathbf{B}^T \mathbf{r}$$

and R_c is a scalar,

$$R_c = \frac{\mathbf{c}^T \mathbf{B}^T \mathbf{r}}{|\mathbf{c}|}.$$

References

- Bischof C, Carle A, Corliss G, Griewank A and Hovland P 1992 *Sci. Programming* **1** 1
 Bishnu P S, Hamiroune D, Metghalchi M and Keck J C 1997 *Combust. Theory Modelling* **1** 295
 Blasco J A, Fueyo N, Dopazo C and Chen J-Y 2000 *Combust. Theory Modelling* **4** 61
 Bodenstein M and Lind S C 1906 *Z. Phys. Chem.* **57** 168
 Caracotsios M and Stewart W E 1985 *Comput. Chem. Eng.* **9** 359
 Chen J-Y, Kollmann W and Dibble R W 1989 *Combust. Sci. Technol.* **64** 315
 Gordon G H and McBride B J 1994 *Computer Program for Calculation of Complex Chemical Equilibrium Compositions and Applications* (NASA Reference Publication) p 1311
 Hamiroune D, Bishnu P, Metghalchi M and Keck J C 1998 *Combust. Theory Modelling* **2** 81
 Keck J C 1990 *Prog. Energy Combust. Sci.* **16** 125

- Keck J C and Gillespie D 1971 *Combust. Flame* **17** 237
- Li G Y, Rosenthal C and Rabitz H 2001 *J. Phys. Chem. A* **105** 7765
- Maas U and Pope S B 1992 *Combust. Flame* **88** 239
- Maas U and Warnatz J 1988 *Proc. Combust. Inst.* **22** 1695
- Nafe J and Maas U 2002 *Combust. Flame* **6** 697
- Peters N and William F A 1987 *Combust. Flame* **68** 185
- Pope S B 1997 *Combust. Theory Modelling* **1** 41
- Pope S B 2004 Gibbs function continuation for the computation of chemical equilibrium *Combust. Flame* submitted
<http://mae.cornell.edu/~pope/Reports/index.html>
- Reynolds W C 1986 *The Element Potential Method for Chemical Equilibrium Analysis: Implementation in the Interactive Program STANJAN* Mechanical Engineering Department, Stanford University
- Smith G P *et al* 1999 http://www.me.berkeley.edu/gri_mech/
- Smooke M D (ed) 1991 *Reduced Kinetic Mechanisms and Asymptotic Approximations for Methane–Air Flames* vol 384 (Berlin: Springer)
- Sung C J, Law C K and Chen J-Y 2001 *Proc. Combust. Inst.* **27** 295
- Tang Q 2003 Computational modelling of turbulent combustion with detailed chemistry *PhD Thesis* Cornell University
- Tang Q and Pope S B 2002 *Proc. Combust. Inst.* **29** 1411
- Tang Q, Xu J and Pope S B 2000 *Proc. Combust. Inst.* **28** 133
- Tomlin A S, Turányi T and Pilling M J 1997 *Comprehensive Chemical Kinetics 35: Low-Temperature Combustion and Autoignition* (Amsterdam: Elsevier)
- Tonse S R, Moriarty N W, Brown N J and Frenklach M 1999 *Israel J. Chem.* **39** 97
- Turányi T 1994 *Comput. Chem.* **18** 45
- Yousefian V 1998 *Combust. Flame* **115** 66